Advanced Composites and Hybrid Materials (2024) 7:41
https://doi.org/10.1007/s42114-024-00855-0

RESEARCH

Transforming oil waste into highly conductive composites: Enabling flexible electronics through laser processing of asphaltenes

Ilia Petrov[1] · Raul D. Rodriguez[1] · Evgeniya Frantsina[2,3] · Andrey Grinko[3] · Evgeniya Sheremet[1]

Received: 10 October 2023 / Revised: 5 February 2024 / Accepted: 13 February 2024

Abstract

Carbon-polymer composites are promising materials in flexible electronics. Nevertheless, they have limitations either in conductivity or in mechanical stability. In this work, we investigate the formation mechanism, properties, and applications of a novel highly conductive and robust composite material, namely, laser-processed asphaltenes with polyethylene terephthalate (LAsp/PET). The composite was formed by the interaction of laser energy with asphaltenes and PET, creating a new material with unique properties. We employed various characterization techniques, including electrical characterization using the 4-point probe method, X-ray photoelectron spectroscopy (XPS), Raman spectroscopy, Fourier-transform infrared spectroscopy (FTIR), and scanning electron microscopy (SEM), to investigate the LAsp/PET material. The characterization results revealed the successful formation of a composite material with excellent electrical conductivity and homogeneity. The XPS analysis confirmed the presence of carbon, oxygen, and nitrogen atoms in the composite material, indicating the successful incorporation of asphaltenes with PET. Raman spectroscopy revealed the characteristic vibrational modes of both asphaltenes and PET, confirming the composite material formation. FTIR analysis further supported the composite nature of LAsp/PET, revealing the presence of various functional groups. Furthermore, we investigated the electrochemical, electrothermal, and mechanical properties of LAsp/PET demonstrating its potential as an electrode material for deformation sensors, electrothermal heaters, electrochemical sensors, supercapacitors, and antennas. Our results indicate that laser processing is an effective method for forming new composite materials with unique properties for various applications.

Keywords Asphaltenes · Oil waste recycling · Flexible electronics · Composite · Photonic processing · Energy storage

1 Introduction

According to the U.S. Energy Administration, since 2006, oil production has been in stable growth, leading to a concerning oil waste accumulation from the oil and gas industry, such as oil sludge, produced wastewater, drilling fluids, and flue gasses [1]. Asphaltenes are heavy heteroatomic components that can make up to 10% of oils and even higher percentages in natural bitumen, fuel oils, tars, and other oil residues [2]. Unfortunately, most of this waste is still being disposed of without any recycling, which is neither environmentally nor economically optimal [1, 3]. Developing a simple, eco-friendly, universal, and scalable recycling technology could solve this issue in a sustainable and economical way, saving millions of dollars on building waste dumps.

Several methods have been proposed for oil waste processing [4–7], including polymer modification and the synthesis of carbonaceous materials. For instance, plasma treatment of asphaltenes resulted in graphitization with the formation of nanotubes, nano-onions, graphene, ultrafine carbon, and carbon nanotubes [8–11]. Asphaltenes as a polymer filler improve mechanical properties [12], thermal stability [12, 13], viscosity, and dynamic modulus [14]. Melamine-activated asphaltenes increased the electrode surface area with implications in capacitor applications [15]. The polyaromatic hydrocarbon structure of asphaltenes is similar to nanographene [16, 17]. However, previous attempts to convert asphaltenes

✉ Raul D. Rodriguez
raul@tpu.ru

[1] Research School of Chemistry & Applied Biomedical Sciences, Tomsk Polytechnic University, Tomsk 634050, Russia

[2] Department of Chemical Engineering, Tomsk Polytechnic University, Tomsk 634050, Russia

[3] Institute of Natural and Technical Sciences, Surgut State University, Surgut 628412, Russia

Published online: 27 February 2024

to graphene using thermal annealing have limitations due to the high temperatures required, often exceeding 500 °C. This limitation restricts the options of substrates that can be used and increases energy costs. Compared to this, laser processing is a scalable and inexpensive technology that allows surface modification with necessary patterning. It was also applied to modify heavy hydrocarbons [18]. Zang et al. showed changes in electrical properties by laser processing of tar, coal, and carbon mesophase on glass. They observed the dehydrogenation of hydrocarbons and identified the critical role of aliphatic chains in generating graphitic structures with π-π stacking. Additionally, they proposed an alternative mechanism for the electrical conductivity between asphaltene molecules due to oxygen cross-linking. Laser processing has many advantages over other methods, including scalability, free-form patterning, and low cost. This makes it an attractive technology for heavy industries like oil production and processing. Furthermore, laser processing provides surface patterning with the desired geometry and conductivity to match specific applications that are impossible to achieve with thermal annealing and other conventional methods [19].

In addition, a laser-based approach makes it possible to use a wide range of materials as the substrate, including glass, polymers, metals, and ceramics. Unlike thermal annealing, plasma, and chemical treatments, laser processing provides precise control of surface modification without affecting the bulk structure of the substrate material. This point is crucial because the substrate partly determines the properties of the processed material. We have shown that different nanomaterials form a composite with polyethylene terephthalate (PET) substrate under laser irradiation [20, 21]. This composite is robust, flexible, and conductive, while the same nanomaterials deposited on glass could be easily washed away. Moreover, polyethylenes are widespread carbon-rich polymers that could act as a carbon source and be recycled for reuse in various applications [22, 23].

Besides, we already investigated plasma-treated asphaltene transformations [11]. In this work, we combine two branches and show heavy hydrocarbon waste recycling using laser processing, achieving record-high levels of electrical conductivity (~ 7000 $S \cdot m^{-1}$) with a material areal capacity of 3.45 mF/cm^2. Also, we explore new applications not shown before with this laser processing/integration technology like Wi-Fi antenna with VSWR = 1.3. In addition, we demonstrate the versatility of our approach using asphaltenes from three different sources as well as asphalts.

2 Experimental

2.1 Asphaltene preparation

The asphaltenes were isolated using a standard procedure described in the literature [6]. Briefly, 40:1 (v.) *n*-hexane was added to the oil sample, and the mixture was kept during the day. Then, the precipitated crude fraction of asphaltenes was purified from maltenes in a Soxhlet apparatus with hexane for 1 day. The resulting asphaltenes were vacuum-dried to constant weight and stored in the dark. Asphaltenes were isolated from the naphthenic oil of the Usinskoye oilfield (marked as UA), from the paraffin-naphthenic oil of the Krapivinskoye oilfield (marked as KA), and from the naphthenoaromatic oil of the Karmalskoye oilfield (marked as KM). The properties of the separated asphaltenes are given in the works [24–26].

2.2 Asphalt preparation

Technological asphalt of an industrial solvent deasphalting plant (SDA process) was used as is.

2.3 LAsp/PET fabrication

LAsp/PET fabrication was performed in the following way: First, asphaltenes with a 20 mg/mL concentration were sonicated in toluene for 10 min. Then, asphaltene/toluene solution was drop cast on a 0.65-mm-thick PET sheet at 50 °C. The areal density of the coating was 50 µL/1 cm^2 of the substrate. After drying, the second layer of asphaltene solution was drop cast at the same conditions. The thickness of the double layer was 20 µm as determined by cross-sectional SEM. Laser processing was done using a 3 W computer-controlled pulsed 438 nm laser. The beam size was 150×350 μm^2, pulse energy 160 mJ, pulse frequency 2.8 kHz, and pulse duration 170 µs. Finally, the samples were washed with toluene in a 120 W ultrasound bath for 2 min.

2.4 Thermogravimetry

Thermogravimetry was carried out by differential thermal analysis (Mettler Toledo TGA/DSC 3+ Star System, heating rate 10 °C/min in the temperature range within 30−1050 °C) in an inert medium (nitrogen).

2.5 Specific capacitance

Specific capacitance was measured using a three-electrode cell with potentiostat/galvanostat P-45X with FRA-24 M impedance modulus (Electrochemical Instruments, Russia). We used Pt and Ag/AgCl electrodes as counter and reference. LAsp/PET, with a surface area of 1.1 cm^2, was used as the working electrode. The potential window was from − 1.5 to 1.5 V at a 100 mV/s scan rate.

2.6 Sheet resistance and impedance

Sheet resistance and impedance were measured using a 4-point probe measurement method. We used potentiostat/galvanostat P-45X with FRA-24 M impedance modulus (Electrochemical Instruments, Russia) in galvanostatic mode and MST 4000A microprobe station (MS Tech, Korea). Probes were set at a square with a 700 μm side. For sheet resistance measurement, the current of 1 mA was applied along one side of a square, and potential was measured along the parallel side. Sheet resistance values were calculated using the following Eq. (1):

$$R = \frac{2\pi}{\ln 2} \cdot \frac{V}{I} \quad (1)$$

where R is the sheet resistance, V is the measured voltage drop, and I is the applied current. The value presented in the text is the average value from three samples with the standard error. For the impedance measurements, the applied voltage was 30 mV in the frequency range of 0–50 kHz.

2.7 Raman spectra

Raman spectra were collected using confocal Raman microscopy (NTEGRA Spectra). A 532 nm laser was used for sample characterization using a × 20 objective. Exposure time was equal to 30 s for PET and 10 min for both Asp/PET and LAsp/PET. Laser power was 4.3 mW for PET and 30 μW for Asp/PET and LAsp/PET.

2.8 Scanning electron microscopy

Scanning electron microscopy images were obtained using Quanta 200 3D, FEI.

2.9 X-ray photoelectron spectroscopy

X-ray photoelectron spectroscopy was performed using a Thermo Fisher Scientific XPS NEXSA spectrometer with a monochromated Al K Alpha X-ray source working at 1486.6 eV. The survey spectra were recorded with the pass energy of 200 eV and energy resolution of 1 eV. For the high-resolution spectra, pass energy was 50 eV, and energy resolution was equal to 0.1 eV. The spot area was 400 μm^2. A flood gun was used to compensate for sample charging.

2.10 FTIR

FTIR spectra were collected in transmission mode using IRAffinity-1S (Shimadzu, Japan) FTIR spectroscope with the scan step of 2 cm^{-1}.

2.11 X-ray diffraction

X-ray diffraction patterns were obtained with Discover D8 (Bruker, Germany) X-ray diffraction spectrometer based on CuKα radiation (λ = 0.154184 nm).

2.12 The bending test

The bending test was performed using a three-point flexural test. A 40 × 10 mm^2 engraved stripe-shaped sample was used. The middle point movement was controlled by a micro-step motor, and the resistance values were measured using a potentiostat/galvanostat P-45X. The constant current of 2 mA was applied to the sample, and a voltage drop during bending cycles was measured. The bending radius was set up to 3, 5, and 7 mm. The bending frequency was 3.7 Hz.

2.13 Electro-heating properties

Electro-heating properties were investigated using a 60 × 60 pixels camera HT-02 from Hit (China) operating at a 30 cm distance from the sample. Operating voltages were in the range of 0–4 V.

2.14 Electrochemical performance

Electro-heating properties were used to detect $K_4Fe(CN)_6$ in an aqueous solution with a 0.1 M concentration in the potential window from − 1 to 1.5 V and a scan rate from 10 to 150 mV /s^{-1}.

2.15 Gel supercapacitor

Gel supercapacitor electrodes were fabricated by laser patterning of a template with a 4.7 cm^2 surface area. Electrolyte gel was fabricated by stirring 0.5 g of PVA in 5 mL of distilled water at 90 °C for 2 h, followed by adding 0.5 mL of phosphoric acid and stirring for 2 h. Electrical contacts were made of copper tape and covered with silver paste. Testing of the supercapacitor was done with potentiostat/galvanostat P-45X with FRA-24 M impedance modulus (Electrochemical Instruments, Russia).

2.16 Wi-Fi antenna

Wi-Fi antenna was fabricated with the size of dipoles equal to 20 × 10 mm^2 and a gap of 4 mm between them. The SMA connector was joined with silver paste and fixed with epoxy on the backside of the antenna. The S_{11} parameter was measured with ARINST VNA-DL 1–8800 MHz vector network analyzer (Arinst, Russia). The antenna was designed by using CAD drawing software.

3 Results and discussions

3.1 Laser processing

The concept developed in this work is illustrated in Fig. 1. Asphaltenes consist of aromatic and naphthetic rings, along with aliphatic chains, and contain carbon vacancies (heteroatoms) that can be occupied by sulfur, antimony, nitrogen, or oxygen or be present in functional groups. As a carbon material, asphaltenes could be used for laser-induced graphene (LIG) production on PET surfaces. Asphaltene films on PET (Asp/PET) act as a photothermal converter, with simulations showing that it can generate surface heating up to 1000 °C under laser irradiation, exceeding the temperature required for LIG formation [27, 28]. This high temperature, coupled with photochemical reactions, triggers various processes, including functional group removal, oxidation, dehydrogenation, elimination of sulfur and nitrogen heteroatoms, and reconstruction of the initially disordered hydrocarbon molecules to a graphene-like lattice. Additionally, the high temperature of Asp/PET can initiate polymer carbonization and melting starting from 240 °C [29]. The localized and fast nature of pulsed laser treatment provides unique and extreme processing conditions, with a 50×50 μm^2 laser spot drastically increasing the temperature and cooling down to room temperature in less than 1 s. Several processes occur within this short period in the laser spot, including graphene formation, polymer melting combined with carbonization, mixing of the two components, and consolidation after cooling. This results in the formation of a robust, flexible, and highly electrically conductive composite of laser-processed asphaltenes with PET (LAsp/PET).

3.2 Characterization

3.2.1 Electrical properties

The electrical properties of a material are crucial for its application in flexible electronics. The experimental procedure for the sample preparation is outlined in Sect. 2.5 and 2.6. We found that the areal capacitance of LAsp/PET in 0.1 M KCl solution is 3.45 mF/cm^2, comparable to the state-of-the-art for laser-reduced GO [30]. We also measured the sheet resistance (R_{sheet}) of LAsp/PET following the method reported in the literature [31]. The sheet resistance for LAsp/PET based on different types of asphaltenes ranged from 2–9 Ohm/sq (UA asphaltenes: (6.6 ± 0.1) Ohm/sq, KA asphaltenes (8.4 ± 0.1) Ohm/sq, KM asphaltenes (3.5 ± 0.6), and their mixture (6.7 ± 0.4) Ohm/sq). We converted the lowest sheet resistance into conductivity based on the thickness of LAsp/PET measured with SEM. The conductivity of up to ~ 7000 S·m^{-1} is comparable to the highest conductivity obtained for laser-reduced GO [32]. These results indicate that the LAsp/PET material is highly conductive, and thus, it warrants further investigation. We investigated the influence of laser power and coating thickness on the electrical properties of LAsp/PET and the surface evolution under different laser regimes (Fig. S1). We found that electrical conductivity could be achieved in a range of laser pulse energies of 115–325 mJ. Increasing the laser power to 325 mJ improved the staking and intermixing of graphene clusters formed by laser pulses. Further increasing the power launched a destructive regime, resulting in material ablation and the formation of blank patches on PET. Also, we optimized the coating thickness to provide the best conductivity. The deposition of 2 asphaltenes layers supplies enough material for modification and provides the best carbonization reflected

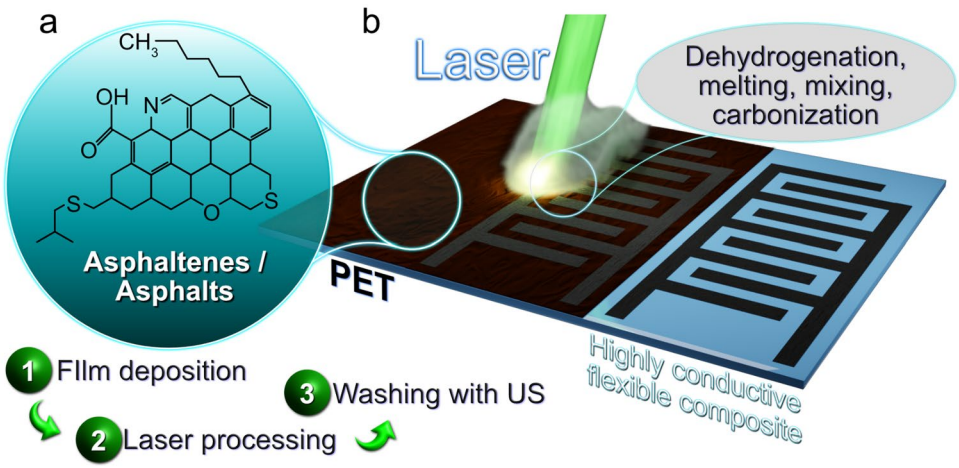

Fig. 1 The concept of the work. **a** Asphaltenes/asphalts chemical structure. **b** Laser processing technology of Asp/PET

in the lowest sheet resistance ((13.1 ± 2.5) Ohm/sq is for 1 layer deposition, and (3.5 ± 0.6) Ohm/sq is for 2-layer deposition). Adding one more layer of asphaltenes reduces the laser-induced coating-substrate interface interaction that results in higher sheet resistance (6.9 ± 2.1) Ohm/sq.

To estimate the spot temperature during laser processing, we performed thermogravimetric analysis (TGA) of asphaltene powder (KM fraction). Fig. S2 reveals that the asphaltene combustion temperature is 443 °C. This point can be associated with the start of thermal modification. Since the photoconversion mechanism is negligible for the 440 nm laser [33], we assume that the LAsp/PET spot temperature exceeds 443 °C.

We also investigated the use of asphalts, a waste product of the solvent deasphalting process that requires less processing for its extraction than asphaltenes [34]. We kept the fabrication protocol the same, and the R_{sheet} of laser-processed asphalt film on PET was (13.9 ± 1.2) Ohm/sq. The similarity in sheet resistance for hydrocarbons with different compositions and structures confirms the versatility of the laser processing approach for any kind of asphaltenes or asphalts and the generality of the processes that occur during laser treatment. In addition, we investigated the impedance of LAsp/PET. The frequency dependence of the material, as shown in Fig. S3, is insignificant, indicating that the capacitance and inductance of the structure are low. To elucidate the impact of the substrate, we repeated the laser processing of asphaltenes on a glass coverslip (LAsp/glass). The sheet resistance of LAsp/glass prepared under the same conditions was (1.5 ± 0.7) MOhm/sq, which exceeds the R_{sheet} values for LAsp/PET by a factor of 105. This strong dependence on the substrate raises the question of what mechanisms occur during laser processing to lead to the extremely high conductivity of the carbon-polymer composite.

3.2.2 Raman spectroscopy and SEM

Raman spectroscopy is a straightforward non-destructive analytical technique that can positively identify and characterize elemental carbon from the shape and position of the bands in the spectrum [35]. In this study, we used Raman spectroscopy to analyze changes in the chemical structure of our samples, as shown in Fig. 2(a). The Raman spectrum of PET is characterized by a set of sharp peaks located at 1726, 1614, 1289, and 1113 cm^{-1} assigned to C = O, carbon ring mode, ester C(O)–O, and ethylene glycol C–C bond vibrations, respectively [36]. The spectrum of Asp/PET displays sharp G and broad D peaks near 1596 and 1346 cm^{-1}. The chemical structure and analysis of asphaltene Raman spectra are complicated. For example, work [37] demonstrated that the deconvolution of the 1st-order carbon region could be done using 3 to 8 Gaussian peaks. Regardless of the fitting applied, the nanocrystallite domain size estimated from the Raman spectra lies within the 1.2–1.6 nm range. Besides the two conventional D and G peaks ($I_D/I_G = 0.6$), we observed two shoulders around the D peak near 1416 and 1283 cm^{-1}. Such shoulders are typical for organic materials with complex structures rather than amorphous carbon, which confirms the presence of functional groups and complexity of the asphaltenes. These D peak shoulders could also be attributed to hetero-atom doping (S, N, O) of the carbon structure [38]. The right shoulder could reflect active modes of CH_n groups in organic compounds [39]. Moreover, these shoulders could be measurement artifacts

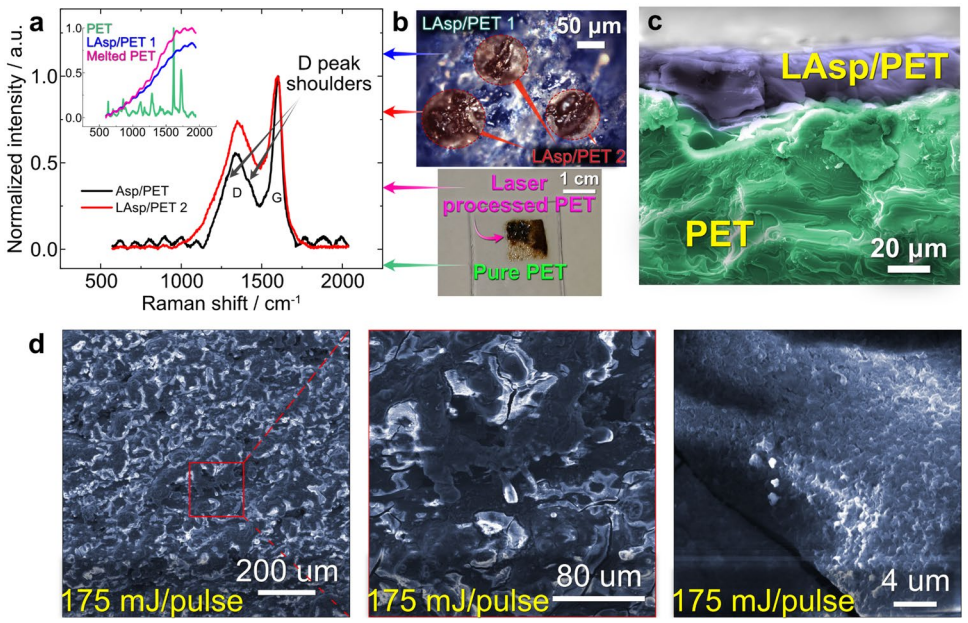

Fig. 2 Characterization of material. **a** Raman spectra of PET, melted PET, Asp/PET, LAsp/PET. **b** optical images of LAsp/PET and 1 × 1 cm^2 laser-processed PET. **c** SEM image of LAsp/PET in cross-section. **d** SEM images of LAsp/PET surface

reflected as periodic patterns through the spectrum. Laser processing significantly modifies the material according to the Raman spectra in Fig. 2(a), transforming a smooth Asp/PET surface to a rough LAsp/PET surface (Fig. 2(b)). Using optical images and Raman spectroscopy, we identified two different regions: bright and highly reflective (LAsp/PET 1) and dark (LAsp/PET 2) marked in Fig. 2(b). The Raman spectrum of LAsp/PET 1 shows high fluorescence, like the spectrum of melted PET processed using higher laser power (see inset). This spectroscopy result confirms the composite formation mechanism suggested before by mixing LAsp with PET.

The Raman spectrum of LAsp/PET 2 shows the D and G peaks, with an increased I_D/I_G ratio of 0.74, indicating a highly defective structure without the second-order peaks. The final confirmation of the composite formation was provided by scanning electron microscopy (SEM) imaging of the cross-section and the surface of the sample (Fig. 2(c), (d)). The cross-section shows two different color-coded regions with a composite depth of about 20–30 µm. The microscale surface of LAsp/PET is highly porous, consisting of ~ 1 µm flakes forming agglomerates. The survey image shows 10–80 µm regions with bright (charged) spots. We attribute these regions to the "asphaltene-poor" polymer with relatively low conductivity. Their formation could be explained by substrate melting with further heat transfer from the underlayer during laser processing.

3.2.3 XPS

After comparing the Raman spectra and electrical measurement results, we needed clarification about how the highly defective structure could achieve such excellent conductivity. We performed X-ray photoelectron spectroscopy (XPS) analysis to investigate this further. The survey XPS spectra of Asp/PET and LAsp/PET are shown in Fig. S4. We found Si, Cl, S, N, and Sb components and dopants of the asphaltenes used in our study, while Na traces come from impurities. Cl originates from the solvent residues (chloroform) used to improve adhesion to PET when preparing samples for XPS. Atomic percentages of Asp/PET and LAsp/PET components based on XPS data are presented in Table S1. We also found that laser irradiation removes silicon, sulfur, and nitrogen from the material structure, while the antimony dopant stays on the surface but gets partially reduced. Antimony peaks Sb_2O_5 $3d_{3/2}$ and Sb_2O_5 $3d_{5/2}$ are located at 540.0 and 530.6 eV for Asp/PET and 540.4 and 531.0 eV for LAsp/PET. The bands of SbO_3 $3d_{3/2}$ and SbO_3 $3d_{5/2}$ are observed at 539.3 and 529.9 eV for LAsp/PET. The deconvoluted Asp/PET spectrum in the C1s region (Fig. 3a) is represented by O–C = O (289.2 eV), C–O–C (286.2 eV), C–C (284.8 eV), and π–π* (290.8 eV) bonds. After laser processing (Fig. 3b), we see the same bonds: O–C = O at 288.8 eV, C–O–C at 286.4 eV, C–C at 284.0 eV, and π–π* bond at 290.7 eV. C–C band shape

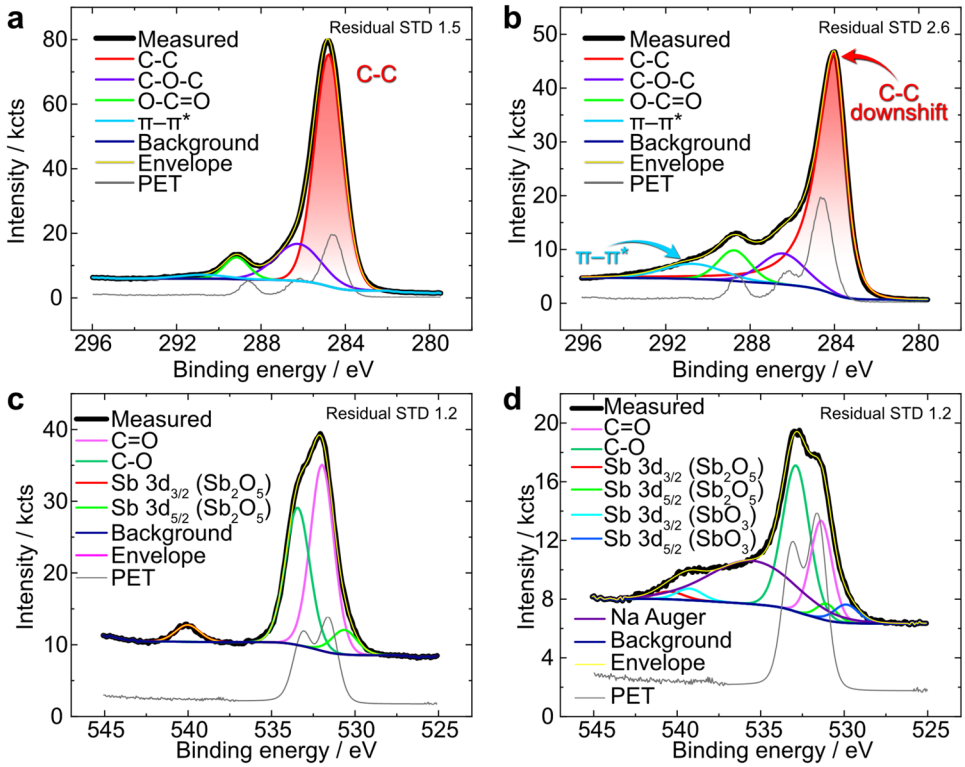

Fig. 3 XPS spectra with reference to8 PET: **a** C1s region spectrum of Asp/PET, **b** C1s region spectrum of LAsp/PET, **c** O1s region spectrum of Asp/PET, **d** O1s region spectrum of LAsp/PET

transforms to a graphite-like peak and significantly downshifts from 284.8 to 284.0 eV. These changes, along with the increasing π–π* bond, explain the high conductivity of the material.

We detected two forms of oxygen in the samples: oxygen with C–O bonding attributed to heteroatoms in the carbon ring and hydroxyl groups. Additionally, we observed C = O bonding, which is assigned to carbonyl groups attached to aliphatic chains. XPS spectra of the O1s region for Asp/PET (Fig. 3c) and LAsp/PET (Fig. 3d) show the material's reconstruction. Initially, the content of the C = O bond (at 532.0 eV) dropped from 50.0 to 35.4%, confirming the removal of carbonylic and carboxylic groups. The content of the C–O bond (at 532.8 eV) slightly decreased from 38.3 to 35.4%. Furthermore, we found a broad peak (at 535.5 eV) in the O1s region that could be assigned to contamination by sodium [40] (Na Auger line may be observed even if Na1s is not in the case of carbon shielding).

3.2.4 FTIR

To investigate whether other factors induced by the substrate play a role in the formation of the highly conductive composite, we performed Fourier-transform infrared spectroscopy (FTIR) of pure PET and PET laser-processed at maximum power (LPET). The spectra in Fig. 4a showed a new band in LPET at 1646 cm^{-1} that corresponds to the C = C bond in alkenes [41]. Previous studies [18] have shown that alkanes supply carbon to aromatic clusters, promoting the formation of graphene-like structures. We hypothesize that alkenes play the same role due to their structural similarity.

Since the sp^3–sp^2 carbon transition is attributed to the dehydrogenation process, we also analyzed the FTIR spectra to confirm hydrogen removal in Asp/PET and LAsp/PET samples (Fig. 4b, c). The IR peak assignment (Table S2) was performed based on previous works [42–44]. The LAsp/PET sample displayed modes of asphaltene and PET. To better understand the changes, we classified them according to

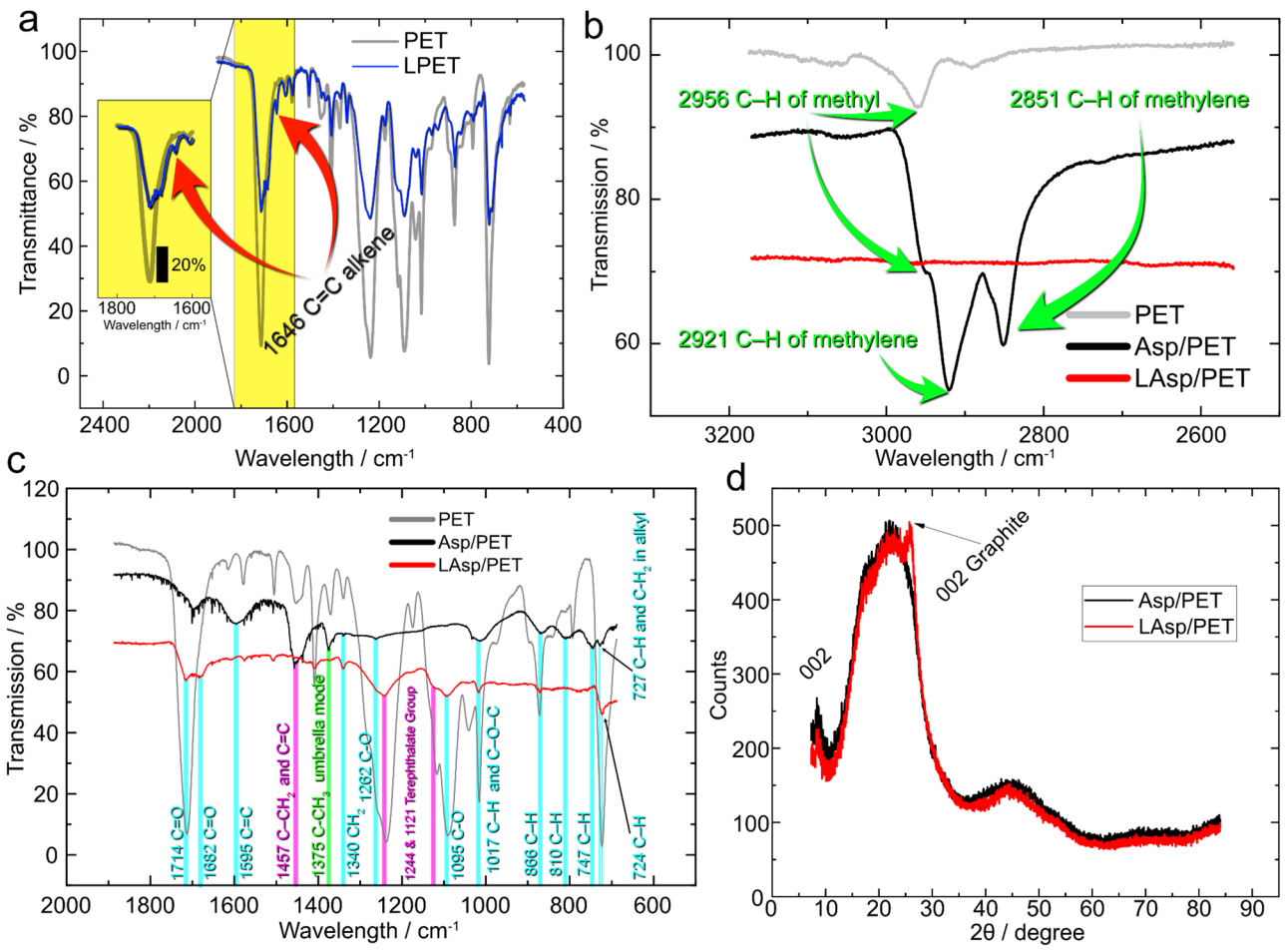

Fig. 4 Materials modification: **a** FTIR spectra of PET and laser-processed PET, **b** FTIR spectra in the range of 2600–3200 cm^{-1} verifying the hydrogenation, **c** FTIR spectra in the range of 600–1900 cm^{-1} revealing structural changes, **d** XRD patterns of Asp/PET and LAsp/PET

the structural components of the sample, namely, aliphatic chains, aromatic rings, and those that could be assigned to both of them. The IR peaks are colored green, cyan, and pink, respectively.

3.2.4.1 Aliphatic chains We observed significant changes in the CH region (2800–3000 cm^{-1}) and found complete removal of C–H methylene groups after laser processing. The disappearance of the band at 1375 cm^{-1} ($C–CH_3$ umbrella mode) also supports this conclusion. These modifications confirm the destruction of aliphatic chains and their reconstruction into other compounds.

3.2.4.2 Aromatic rings In LAsp/PET, we observed a new band at 1682 cm^{-1} (C = O mixed ketones). The band at 1595 cm^{-1} (C = C in aromatics) decreased, while the trans-wagging band of $–CH_2$ at 1340 cm^{-1} increased. The band at 1095 cm^{-1} could be assigned both to the methylene group and the vibrations of the ester C–O bond. Since we do not observe any methylene vibrations in the 2800–3000 cm^{-1} region, we assume this bond is completely related to the C–O–C (ester) vibration in the composite. The bands of C–H in adjacent hydrogen aromatic rings in the range of 810–727 cm^{-1} disappeared, confirming dehydrogenation. We see bands at 724 and 870 cm^{-1} in the LAsp/PET spectrum, which can be assigned to the interaction of polar ester groups, benzene rings, and aromatic rings 1, 2, 4, and 5 (tetra replaced).

3.2.4.3 Changes in chains and aromatics The band at 1457 cm^{-1} ($C–CH_2$ and C = C in aromatics) disappeared, and bands at 1244 and 1121 cm^{-1} (terephthalate group [$OOCC_6H_4–COO$]) appeared, which could be assigned to the PET matrix of LAsp/PET.

The changes observed in chemical structure may explain the conductivity changes we evidenced. Previous studies on polymer composites with conductive fillers showed that the resistance is determined by two primary mechanisms: ohmic resistance for a well-connected network of conductive particles and hopping/tunneling between conductive particles [45]. Therefore, the improved conductivity of the LAsp/PET system compared to the LAsp/glass system could be explained by several mechanisms: improved formation of the conductive network in PET, which is typical for polymers with polar groups [46], PET carbonization during laser annealing, or an improved hopping rate through different connectors such as C–O–C bridges, as compared to particles isolated by thin polymer layers [47]. Given that the resistance of LAsp/PET is comparable to that of graphite and the frequency dependence is low (Fig. S3), it is reasonable to assume that the ohmic conduction through graphene-like particles dominates the electronic transport in this material [48].

3.2.5 XRD

The XRD pattern of Asp/PET (shown in Fig. 4d) exhibits a sharp peak near 2θ = 10° and a broad peak near 2θ = 22°, both of which are assigned to the graphite structure in the (002) orientation. A sharp peak at 10° is attributed to oxygen functionalities in carbon [49], while the broad peak at 22° indicates that the asphaltene has a π-conjugated structure, with the crystal phase (002) randomly arranged [50]. LAsp/PET has a similar pattern, but one sharper peak can be observed near 2θ = 26°. This peak confirmed the presence of an arranged graphite structure along the (002) orientation. The broad peak near 44° is attributed to the turbostratic band of disordered carbon materials in the (001) orientation and is observed in both Asp/PET and LAsp/PET samples.

3.3 Applications

LAsp/PET combines high conductivity and robustness. These properties are essential in flexible electronics, especially in the ones of the most interesting branches as flexible sensors, energy storage, and communication [51, 52]:

- Mechanical and chemical stability are significant for electrochemical sensors and body-machine interfaces to function in an aggressive environment and operate as actuators, motion sensors, etc.
- Low resistivity allows the fabrication of effective electric heaters and matched antennas with smaller sizes.
- The rough surface of the material provides an increased electrode area for electrolytic capacitors.

One of our aims is to design a metal-free electric circuit for sensing. In this section, we propose the electronic elements possible with LAsp/PET with respect to the our goals and material benefits.

3.3.1 Bending sensor

We aimed to explore potential applications that take advantage of the impressive properties of LAsp/PET, for instance, in flexible electronics. To this end, we created a bending sensor using this material, building upon our previous research on the reaction mechanism [20]. The sensor operates based on the elastic deformation-induced changes in intercluster distances within the composite, leading to a change in resistance (Fig. 5a). Upon relaxation, the graphene flakes return to their original position, restoring conductivity. The sensor demonstrates exceptional elastic and resistivity stability, undergoing over 2400 bending cycles with a resistance change of 58, 78, and 174% at bending radii of 3, 5, and 7 mm, respectively.

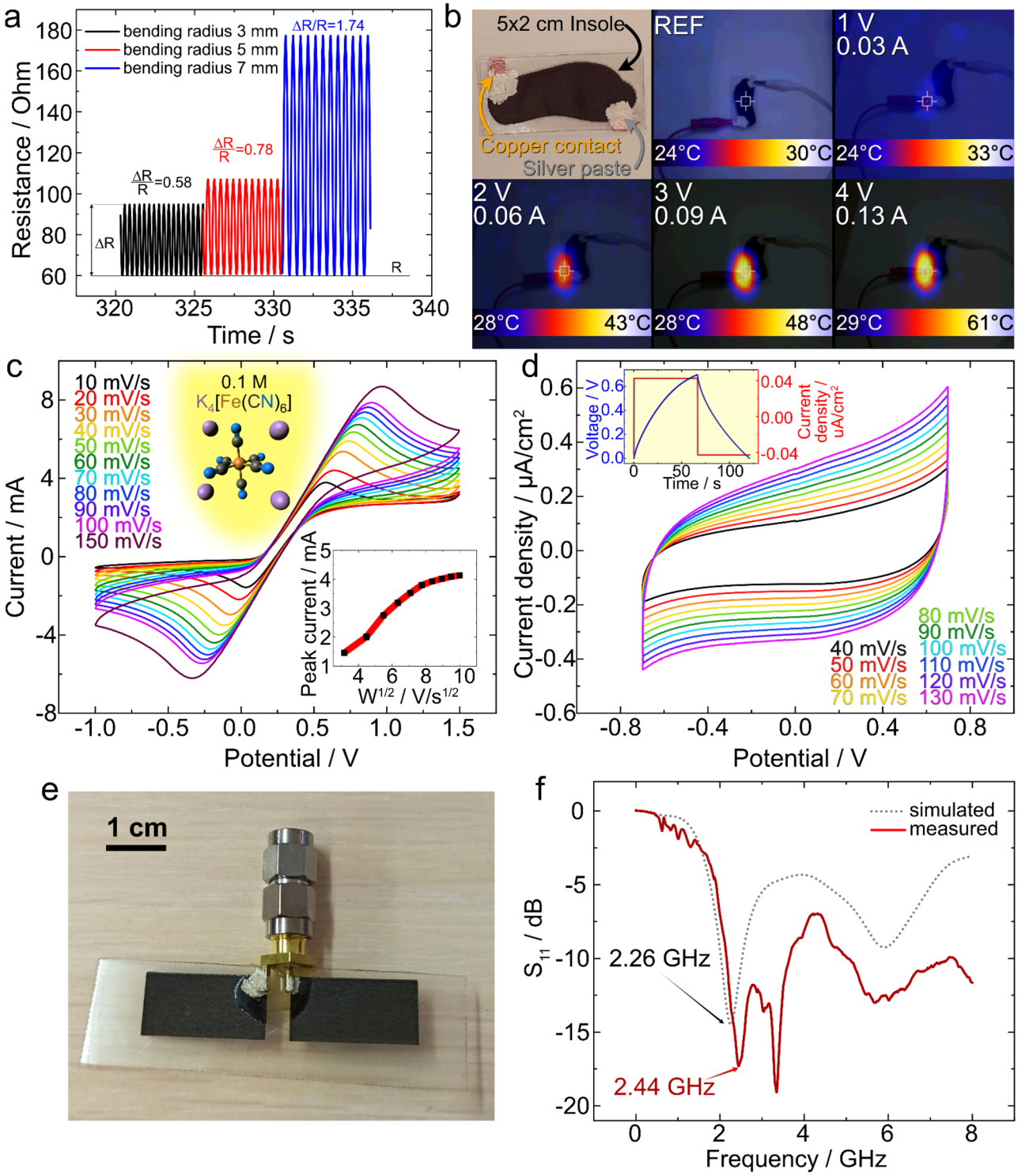

Fig. 5 Applications of LAsp/PET. **a** Resistance changes of the bending sensor during testing. **b** Thermal images of the insole-shaped electrothermal heater at different voltages. **c** Voltammogram of 0.1 M potassium ferrocyanide solution and dependency of peak current on the square root of scan speed (inset). **d** I–V curves of LAsp/PET supercapacitor at different scan rates with the charge-discharge diagram inset. **e** Photo of LAsp/PET 2.4 GHz antenna with SMA adapter. **f** Reflection coefficient of simulated and fabricated antennas

3.3.2 Electrical heater

Given the low sheet resistance of LAsp/PET, we investigated its potential for electro-heating applications. To test this, we created an insole with dimensions of 5×2 cm^2, as shown in Fig. 5b, and made electrical contacts using copper tape with silver paste. We applied different voltages to the sample for 1 min at room temperature and used a thermal camera to map the temperature changes in the sample. The maximum temperature in the region of interest increased from 30 to 48 °C at 3 V and 0.09 A. Increasing the voltage further to 4 V resulted in heating up to 61 °C, which is close to the softening limit of the polymer substrate [53]. The achieved temperature of 61 °C with a current flow at a power of 0.52 W demonstrates promising opportunities for this material in developing multifunctional self-heating clothes.

3.3.3 Electrochemical sensor

Carbon is a popular material in electrochemical electrodes due to its high surface area, corrosion resistance, and low cost, making it attractive for different applications like hydrogen generation or water purification [54]. We investigated LAsp/PET as an electrochemical electrode. For this, we used 0.1 M aqueous potassium ferrocyanide solution as a model analyte system, which is also commonly used as a food additive [55]. The counter electrode was Pt, the reference electrode was Ag/AgCl, and the working electrode was LAsp/PET. We conducted cyclic voltammetry (CV) at different scan rates in the range of (− 1–1.5) V, as shown in Fig. 5c. Following the reaction on the electrode, $[Fe(CN)_6]^{3-} + e^- = [Fe(CN)_6]^{4-}$, the obtained I–V curves showed the characteristic reduction peak of $[Fe(CN)_6]^{3-}$ and the oxidation peak of $[Fe(CN)_6]^{4-}$. The electrode shows stable behavior in the potential window of − 1 to + 1.5 V. Increasing the scanning speed increases mass transport, which is evident by plotting the peak intensity vs. the square root of the scan speed, as shown in the inset of Fig. 5c. The linear fit of the plot with a coefficient of determination (COD) = 0.95 shows fast response dynamics that are not limited by the charge transfer facilitated by the LAsp/PET electrode.

3.3.4 Supercapacitor

Achieving large surface area and efficient charge transfer are critical challenges in the fabrication of supercapacitors [56, 57]. Therefore, we aimed at the fabrication of an interdigitated supercapacitor with LAsp/PET after observing the linear behavior of the current-scan rate curve during potassium ferrocyanide detection. The gel-electrolyte was made of PVA/H_3PO_4. We first tested the supercapacitor using cyclic voltammetry scanning at different speeds in the potential range from − 0.7 to + 0.7 V (Fig. 5d). No reduction or oxidation peaks were observed in this range. However, increasing the potential window resulted in the electrocatalysis of orthophosphoric acid, leading to rapid current increase at higher voltages. The areal capacitance was calculated and averaged for all I–V curves using the formula (1)

$$C = \frac{A}{w \cdot \Delta V \cdot S} \tag{1}$$

where C is the areal capacitance, A is the integrated area of the I–V curves, w is the scan speed, ΔV is the potential window, and S is the surface area of electrodes. The areal capacitance was estimated as (5.1 ± 0.4) μF. Next, we conducted charge-discharge testing at a charge current density of + 0.04 and discharge current of − 0.04 μA to simulate electrical load (inset of Fig. 5d). The charge accumulated on the capacitor plate at 0.7 V was 26.67 μQ which corresponds to a capacitance of 38.1 μF. Notably, the capacitance is tunable by varying electrodes' geometrical parameters, such as their number, length, and width.

We also tested the ability of the supercapacitor to store energy by measuring galvanostatic self-discharge. The discharge curve and photo of the supercapacitor are shown in Fig. S5. We found that the capacitor loses half of the accumulated charge in 11 min and still retains 15% of the accumulated charge after 100 min. Our results demonstrate that LAsp/PET is a promising material for fabricating supercapacitors with high areal capacitance, efficient charge transfer, and exponential discharge behavior. This aligns with the established theory and practical experience of supercapacitors [58].

3.3.5 Wi-Fi antenna

The impressive conductivity and mechanical stability of LAsp/PET allowed us to design and fabricate a full-carbon dipole antenna (Fig. 5e). It was designed to provide a Wi-Fi connection and tuned to 2.4 GHz. The main resonant band of the device corresponds to 2.44 GHz with the − 17.7 dB amplitude and VSWR of 1.3, while S_{11} resonance of the simulated model is located at 2.26 GHz with amplitude of − 14.5 dB and the VSWR of 1.5 (Fig. 5f). Similar parameters of metal-free antennas were obtained with graphene [59–61] and rGO [62] ink which does not fulfill the mechanical stability requirements and limits the possible applications despite the high costs of precursor. Taking it into account, we declare a new low-cost technology of asphaltene-PET laser processing which performance competes with graphene and rGO in RF applications.

4 Conclusions

We investigated a new composite material, LAsp/PET, formed by laser energy interacting with asphaltenes and a polymer substrate (PET). Various characterization techniques

confirmed the successful formation of the composite. We have also shown that LAsp/PET has promising electrochemical, electrothermal, and mechanical properties, making it a potential candidate for various applications, such as deformation sensors, electrothermal heaters, electrochemical sensors, supercapacitors, and antennas. Our approach presents a simple, eco-friendly, and scalable recycling technology for heavy hydrocarbon waste, which could provide a sustainable and economical solution for the oil and gas industry.

Supplementary Information The online version contains supplementary material available at https://doi.org/10.1007/s42114-024-00855-0.

Acknowledgements We thank Prof. Mekhman Yusubov for inspiring this work. The authors thank the central laboratories of TPU (Analytical Center) for the XPS measurements and Oleg Semenov for operating the equipment.

Author contributions I.P. performed sample preparation, sample characterization, and application performance, wrote the main text, and prepared the figures. R.D.R. proposed the idea of the laser processing of asphaltenes and contributed to major text and figure corrections. E.F. synthesized asphaltene powder, provided TGA analysis, and wrote the introduction. A.G. proposed the solvents for sample preparation, synthesized asphalt powder, and wrote the introduction. E.S. was the scientific supervisor of this work, wrote the part Results and discussion, and was in charge of the logic and meaning of the work. All authors reviewed the manuscript.

Funding Financial support on physicochemical characterization and applications was provided by the Priority 2030-NIP/IZ-007–375-2023 project. Work was conducted using the equipment of the Tomsk Regional Core Shared Research Facilities Centre of National Research Tomsk State University.

Data availability The experimental data are available from the corresponding author on reasonable request.

Declarations

Competing interests The authors declare no competing interests.

References

1. Shahbaz M, Rashid N, Saleem J et al (2023) A review of waste management approaches to maximise sustainable value of waste from the oil and gas industry and potential for the State of Qatar. Fuel 332:126220. https://doi.org/10.1016/j.fuel.2022.126220
2. Mu B, Zhu W, Zhong J et al (2021) Mechanism of separation and removal of water from oily sludge using liquid dimethyl ether to dissolve hydrocarbons. Chemosphere 279:130452. https://doi.org/10.1016/j.chemosphere.2021.130452
3. Safiulina AG, Ibragimova DA, Baibekova LR et al (2018) Modeling of paraffin wax deposition process in poorly extractable hydrocarbon stock. Chem Technol Fuels Oils 53:897–904. https://doi.org/10.1007/s10553-018-0879-x
4. Subirana M, Sheu EY (2013) Asphaltenes: fundamentals and applications. Springer Science & Business Media
5. Kamkar M, Natale G (2021) A review on novel applications of asphaltenes: a valuable waste. Fuel 285:119272
6. Boczkaj G, Momotko M, Chruszczyk D et al (2016) Novel stationary phases based on asphaltenes for gas chromatography. J Sep Sci 39:2527–2536. https://doi.org/10.1002/jssc.201600183
7. Saadi MASR, Advincula PA, Thakur MSH et al (2022) Sustainable valorization of asphaltenes via flash joule heating. Sci Adv 8:eadd3555. https://doi.org/10.1126/sciadv.add3555
8. Petrova YY, Frantsina EV, Grin'ko AA, et al (2022) Investigation of the process and products of plasma treatment of asphaltenes. Mater Today Commun 33:104669. https://doi.org/10.1016/j.mtcomm.2022.104669
9. Pak AY, Larionov KB, Kolobova EN et al (2022) A novel approach of waste tires rubber utilization via ambient air direct current arc discharge plasma. Fuel Process Technol 227:107111. https://doi.org/10.1016/j.fuproc.2021.107111
10. Xu K, Li Y, Xu C et al (2013) Controllable synthesis of single-, double- and triple-walled carbon nanotubes from asphalt. Chem Eng J 225:210–215. https://doi.org/10.1016/j.cej.2013.03.096
11. Frantsina E, Petrova Y, Arkachenkova V et al (2023) The influence of composition of asphaltenes of different genesis on the properties of carbon materials manufactured from them by plasma processing. Pet Sci. https://doi.org/10.1016/j.petsci.2023.07.012
12. Siddiqui MN (2015) Studies of different properties of polystyrene-asphaltene composites. Macromol Symp 354:184–190
13. Siddiqui MN, Redhwi HH, Younas M et al (2018) Use of asphaltene filler to improve low-density polyethylene properties. Pet Sci Technol 36:756–764
14. Wu H, Thakur VK, Kessler MR (2016) Novel low-cost hybrid composites from asphaltene/SBS tri-block copolymer with improved thermal and mechanical properties. J Mater Sci 51:2394–2403
15. Enayat S, Tran MK, Salpekar D et al (2020) From crude oil production nuisance to promising energy storage material: development of high-performance asphaltene-derived supercapacitors. Fuel 263:116641. https://doi.org/10.1016/j.fuel.2019.116641
16. Xy C, Ning G, Zhu X et al (2013) Synthesis of graphene from asphaltene molecules adsorbed on vermiculite layers. Carbon N Y 62:213–221. https://doi.org/10.1016/j.carbon.2013.05.059
17. Wu C, Xu Q, Ning H et al (2022) Petroleum pitch derived carbon as both cathode and anode materials for advanced potassium-ion hybrid capacitors. Carbon N Y 196:727–735. https://doi.org/10.1016/j.carbon.2022.05.021
18. Zang X, Jian C, Ingersoll S et al (2020) Laser-engineered heavy hydrocarbons: old materials with new opportunities. Sci Adv 6:eaaz5231. https://doi.org/10.1126/sciadv.aaz5231
19. Kumar R, Pérez del Pino A, Sahoo S et al (2022) Laser processing of graphene and related materials for energy storage: state of the art and future prospects. Prog Energy Combust Sci 91:100981. https://doi.org/10.1016/j.pecs.2021.100981
20. Lipovka A, Petrov I, Fatkullin M et al (2022) Photoinduced flexible graphene/polymer nanocomposites: design, formation mechanism, and properties engineering. Carbon N Y 194:154–161. https://doi.org/10.1016/j.carbon.2022.03.039
21. Rodriguez RD, Shchadenko S, Murastov G et al (2021) Ultra-robust flexible electronics by laser-driven polymer-nanomaterials integration. Adv Funct Mater. https://doi.org/10.1002/adfm.202008818
22. Singh MV, Kumar S, Sarker M (2018) Waste HD-PE plastic, deformation into liquid hydrocarbon fuel using pyrolysis-catalytic cracking with a CuCO3 catalyst. Sustain Energy Fuels 2:1057–1068. https://doi.org/10.1039/c8se00040a
23. Ahangar FA, Rashid U, Ahmad J et al (2021) Conversion of waste polyethylene terephthalate (PET) polymer into activated carbon and its feasibility to produce green fuel. Polymers. https://doi.org/10.3390/polym13223952
24. Grin'ko AA, Golovko AK, (2011) Fractionation of resins and asphaltenes and investigation of their composition and structure

using heavy oil from the Usa field as an example. Pet Chem 51:192–202. https://doi.org/10.1134/S0965544111030066
25. Grin'ko AA, Golovko AK, (2014) Thermolysis of petroleum asphaltenes and their fractions. Pet Chem 54:42–47. https://doi.org/10.1134/S0965544113040051
26. Sviridenko NN, Vosmerikov AV, Agliullin MR, Kutepov BI (2020) General features of catalytic upgrading of karmalskoe heavy oil in the presence of amorphous aluminosilicates. Pet Chem 60:384–391. https://doi.org/10.1134/s0965544120030214
27. Wen L, Zhou T, Zhang J, Zhang A (2016) Local controllable laser patterning of polymers induced by graphene material. ACS Appl Mater Interfaces 8:28077–28085. https://doi.org/10.1021/acsami.6b09504
28. Farazila Y (2011) YAG laser spot welding of PET and metallic materials. J Laser Micro/Nanoeng 6:69–74. https://doi.org/10.2961/jlmn.2011.01.0015
29. Wang L, Wang Y, Zhang F et al (2017) Syntheses and properties of the PET-co -PEA copolyester. J Appl Polym Sci 134:44967. https://doi.org/10.1002/app.44967
30. Hamed A, Hessein A, Abd El-Moneim A (2021) Towards high performance flexible planar supercapacitors: in-situ laser scribing doping and reduction of graphene oxide films. Appl Surf Sci 551:149457. https://doi.org/10.1016/j.apsusc.2021.149457
31. Miccoli I, Edler F, Pfnür H, Tegenkamp C (2015) The 100th anniversary of the four-point probe technique: the role of probe geometries in isotropic and anisotropic systems. J Phys Condens Matter 27:223201. https://doi.org/10.1088/0953-8984/27/22/223201
32. Wang Y, Chen Y, Lacey SD et al (2018) Reduced graphene oxide film with record-high conductivity and mobility. Mater Today 21:186–192. https://doi.org/10.1016/j.mattod.2017.10.008
33. Smirnov VA, Shul'ga, Y.M., Denisov, N.N. et al (2012) Photoreduction of graphite oxide at different temperatures. Nanotechnol Russia 7:156–163. https://doi.org/10.1134/S1995078012020164
34. Cheshkova TV, Sergun VP, Kovalenko EY et al (2019) Resins and asphaltenes of light and heavy oils: their composition and structure. Energy Fuels 33:7971–7982. https://doi.org/10.1021/acs.energyfuels.9b00285
35. Smith E, Dent G (2004) Modern Raman spectroscopy: a practical approach. John Wiley & Sons, Nashville, TN
36. Rebollar E, Pérez S, Hernández M et al (2014) Physicochemical modifications accompanying UV laser induced surface structures on poly(ethylene terephthalate) and their effect on adhesion of mesenchymal cells. Phys Chem Chem Phys 16:17551–17559. https://doi.org/10.1039/c4cp02434f
37. Abdallah WA, Yang Y (2012) Raman spectrum of asphaltene. Energy Fuels 26:6888–6896. https://doi.org/10.1021/ef301247n
38. Kim D-W, Li OL, Saito N (2015) Enhancement of ORR catalytic activity by multiple heteroatom-doped carbon materials. Phys Chem Chem Phys 17:407–413. https://doi.org/10.1039/c4cp03868a
39. Maheswari UJ (2015) Sundius T (2015) Molecular Docking, IR, Raman Studies on Heterocyclic Aromatic Compound. Austin Chem Eng 2(1):1016
40. Zhao N, Li C, Guo X (2014) Long-life Na-O_2 batteries with high energy efficiency enabled by electrochemically splitting NaO_2 at a low overpotential. Phys Chem Chem Phys 16:15646–15652. https://doi.org/10.1039/c4cp01961j
41. Smith BC (2019) The infrared spectroscopy of alkenes. Spectroscopy. https://www.spectroscopyonline.com/view/infrared-spectroscopy-alkenes. Accessed 11 Jan 2024
42. Asemani M, Rabbani AR (2020) Detailed FTIR spectroscopy characterization of crude oil extracted asphaltenes: curve resolve of overlapping bands. J Pet Sci Eng 185:106618. https://doi.org/10.1016/j.petrol.2019.106618
43. Mecozzi M, Nisini L (2019) The differentiation of biodegradable and non-biodegradable polyethylene terephthalate (PET) samples by FTIR spectroscopy: a potential support for the structural differentiation of PET in environmental analysis. Infrared Phys Technol 101:119–126. https://doi.org/10.1016/j.infrared.2019.06.008
44. dos Pereira AP, S, Silva MHP da, Lima Júnior ÉP, et al (2017) Processing and characterization of PET composites reinforced with geopolymer concrete waste. Mater Res 20:411–420. https://doi.org/10.1590/1980-5373-mr-2017-0734
45. Liu H, Li Q, Zhang S et al (2018) Electrically conductive polymer composites for smart flexible strain sensors: a critical review. J Mater Chem 6:12121–12141. https://doi.org/10.1039/C8TC04079F
46. Sau KP, Chaki TK, Khastgir D (1998) Carbon fibre filled conductive composites based on nitrile rubber (NBR), ethylene propylene diene rubber (EPDM) and their blend. Polymer 39:6461–6471
47. Li H, Zhu T, Ferralis N, Grossman JC (2019) Charge transport in highly heterogeneous natural carbonaceous materials. Adv Funct Mater 29:1904283. https://doi.org/10.1002/adfm.201904283
48. Medalia AI (1986) Electrical conduction in carbon black composites. Rubber Chem Technol 59:432–454
49. Cui P, Lee J, Hwang E, Lee H (2011) One-pot reduction of graphene oxide at subzero temperatures. Chem Commun 47:12370–12372. https://doi.org/10.1039/c1cc15569e
50. Thakur S, Karak N (2012) Green reduction of graphene oxide by aqueous phytoextracts. Carbon N Y 50:5331–5339. https://doi.org/10.1016/j.carbon.2012.07.023
51. Wang P, Hu M, Wang H et al (2020) The evolution of flexible electronics: from nature, beyond nature, and to nature. Adv Sci 7:2001116. https://doi.org/10.1002/advs.202001116
52. Corzo D, Tostado-Blázquez G, Baran D (2020) Flexible electronics: status, challenges and opportunities. Front Electron. https://doi.org/10.3389/felec.2020.594003
53. Abyzova E, Petrov I, Bril' I et al (2023) Universal approach to integrating reduced graphene oxide into polymer electronics. Polymers. https://doi.org/10.3390/polym15244622
54. Rana A, Baig N, Saleh TA (2019) Electrochemically pretreated carbon electrodes and their electroanalytical applications – a review. J Electroanal Chem 833:313–332. https://doi.org/10.1016/j.jelechem.2018.12.019
55. Na M, Chen Y, Han Y et al (2019) Determination of potassium ferrocyanide in table salt and salted food using a water-soluble fluorescent silicon quantum dots. Food Chem 288:248–255. https://doi.org/10.1016/j.foodchem.2019.02.111
56. Zhang L, Hu X, Wang Z et al (2018) A review of supercapacitor modeling, estimation, and applications: a control/management perspective. Renewable Sustainable Energy Rev 81:1868–1878. https://doi.org/10.1016/j.rser.2017.05.283
57. Wang Y, Zhang L, Hou H et al (2021) Recent progress in carbon-based materials for supercapacitor electrodes: a review. J Mater Sci 56:173–200. https://doi.org/10.1007/s10853-020-05157-6
58. Frackowiak E (2007) Carbon materials for supercapacitor application. Phys Chem Chem Phys 9:1774–1785. https://doi.org/10.1039/b618139m
59. Akbari M, Khan MWA, Hasani M et al (2016) Fabrication and characterization of graphene antenna for low-cost and environmentally friendly RFID tags. IEEE Antennas Wirel Propag Lett 15:1569–1572. https://doi.org/10.1109/lawp.2015.2498944
60. Wang W, Ma C, Zhang X et al (2019) High-performance printable 2.4 GHz graphene-based antenna using water-transferring technology. Sci Technol Adv Mater 20:870–875. https://doi.org/10.1080/14686996.2019.1653741
61. Colmiais I, Silva V, Borme J et al (2022) Towards RF graphene devices: a review. FlatChem 35:100409. https://doi.org/10.1016/j.flatc.2022.100409

62. Lv S, Ye S, Chen C et al (2021) Reactive inkjet printing of graphene based flexible circuits and radio frequency antennas. J Mater Chem C Mater Opt Electron Devices 9:13182–13192. https://doi.org/10.1039/d1tc0235F2g